Chemistry
Europe
European Chemical
Societies Publishing

www.eurjic.org

Static and Dynamic Magnetic Properties of a Co(II)-Complex with N_2O_2 Donor Set – A Theoretical and Experimental Study

Sunil Kumar,[a] Selvakumar Arumugam,[a] Björn Schwarz,*[b] Helmut Ehrenberg,[b] and Kartik Chandra Mondal*[a]

A representative Co(II) based single ion magnet (SIM) with N_2O_2 donor set and distorted pseudo-tetrahedral geometry has been synthesized and characterized to study the atomic and electronic structure. DC magnetometry results have been evaluated by means of a phenomenological Hamiltonian approach regarding zero field splitting (ZFS) parameters and compared with results from ab-initio multi-reference CASSCF (complete active space self-consistent field) calculations and qualitative ligand field theory (AILFT). Profound investigation of spin-lattice relaxation with the variation of temperature (from 1.8 to about 8 K) and magnetic field (at 14 different fields from zero up to 1 T) have been performed based on AC magnetometry. Under an applied dc magnetic field, spin-lattice relaxation occurs via a direct process with T^2 temperature dependence due to limited heat transfer at very low temperature and above 5 K relaxation by an Orbach process with an energy barrier of $U_{eff} \approx 80$ K dominates.

Introduction

The first single molecule magnet (SMM) Mn_{12}-Ac was discovered in the early 90s[1,2] and since then there has been a considerable amount of research interest in synthesizing and characterizing SMMs. The reason behind is their possible application in high density data storage devices,[3] molecular spintronic devices[4] and quantum computing[5]. The substantial easy-axis or Ising type anisotropy and a high magnetic moment respectively high spin quantum number are essential for the molecule to behave as SMM.[6,7] The magnetic hysteresis loop that appears below the blocking temperature is entirely of molecular origin and is the fundamental property utilized for practical data storage applications.[8] The majority of the reported SMMs however exhibit very low blocking temperatures limiting their practical usability. Until now, the blocking temperature of cationic dysprosium metallocene based mononuclear SMM has been achieved above liquid nitrogen temperature,[9] but SMMs that can be used at room temperature in practical applications have

yet to be realized. Mn-based SMMs[1,2] exhibit slow relaxation of magnetization due to the presence of a strong axial magnetic local anisotropy (often parametrized by the zero-field splitting (ZFS) parameter D) that presents an energy barrier for magnetic reversal from pointing along the easy axis to pointing along the opposite direction.[10] The reversal of spin/magnetization via an energy barrier is accompanied by thermal energy transfer from the spin to the lattice system (and vice versa) called spin-lattice relaxation. The Orbach mechanism, for instance, represents one spin-lattice relaxation mechanism where the relaxation rate τ^{-1} exhibits an Arrhenius type dependence on the energy barrier U_{eff} and temperature T of the form $\tau^{-1} = \tau_0^{-1}\exp(-U_{eff}/k_BT)$. The energy barrier for systems with total spin $S > 1/2$ is given by $U_{eff} = |D|S^2$ (spin giant model with well-defined spin ground state) for non-Kramer systems with integer S and by $U_{eff} = |D|(S^2 - 1/4)$ for Kramer systems with half-integer S in the case that the Orbach mechanism is dominating the spin-lattice relaxation.[11–13] As the energy barrier is proportional to the square of the total ground state spin S, the research concentrated more on increasing the total spin by synthesis of polynuclear ferromagnetically exchange linked magnetic compounds.[14] Later, it was theoretically predicted that increasing S beyond 12 will not further improve the energy barrier since the ZFS D value itself is inversely proportional to S^2 partially because of the random orientation of the easy-axis of magnetization at each magnetic center.[11–13] As a result, research efforts are now preferentially concentrating on increasing the D value of a single ion. The lanthanide ions do have first order unquenched orbital angular momentum and therefore have large single ion magnetic anisotropy. The first lanthanide based mononuclear single ion magnet, possessing substantial magnetic anisotropy due to the contribution of first order orbital angular momentum contribution, was discovered in 2002.[15] As a result, researchers were interested in mononuclear

[a] S. Kumar, S. Arumugam, Prof. Dr. K. C. Mondal
     Department of Chemistry
     Indian Institute of Technology Madras
     Chennai- 600 036 (India)
     E-mail: csdkartik@iitm.ac.in
[b] Dr. B. Schwarz, Prof. Dr. H. Ehrenberg
     Institute for Applied Materials (IAM)
     Karlsruhe Institute of Technology (KIT)
     Hermann-von-Helmholtz-Platz 1
     76344 Eggenstein-Leopoldshafen, Germany
     E-mail: bjoern.schwarz@kit.edu

EurJIC
European Journal of Inorganic Chemistry

Research Article
doi.org/10.1002/ejic.202200774

Chemistry Europe
European Chemical Societies Publishing

single ion magnets, also known as single ion magnets SIM.[16] Till now, lanthanides complexes have been proven to be excellent SIMs due to their large magnetic anisotropies giving rise to high energy barriers and high blocking temperatures.[9,15,16] In many high symmetrically coordinated complexes, the orbital momentum of 3d transition metal ions is quenched by the ligand field symmetry 'firstly' but can partially be restored by (second order) spin-orbit coupling between the ground and excited states[17–19] to again create SIMs with local magnetic anisotropy. Other transition metal ions can preserve their first order orbital angular momentum in low coordination environment, but their theoretical description is more difficult.[17–19] The energy barrier of the SIMs can be increased by properly tuning of the crystal/ligand field and controlling the coordination geometry what is of course a future challenging task in practice. The linear two-coordinated SIMs of high spin Fe(I) and Co(II) ions possess remarkable energy barriers due to the presence of first order orbital angular momentum. But due to their low coordination, they are more air sensitive which may limit their usability in practical applications.[20,21] Among the 3d transition metal-based SIMs, large magnetic anisotropy is known to exist in a significant variety of Co(II) based high spin complexes with varying coordination numbers and geometries.[21,22] Complexes with pseudo-tetrahedral geometries have been investigated extensively and are known to exhibit slow relaxation of magnetization at zero or applied dc fields.[6,23,24–26] But the Co(II) SIMs with zero field relaxation are scarce.[25,26] The fast quantum tunneling of magnetization (QTM) is responsible for the lower number of examples displaying slow relaxation of magnetization at zero field.[27] To create an effective large energy barrier for spin reversal, it becomes necessary to suppress the QTM at zero field. This can be accomplished by proper designing and tweaking the ligand field so that the transverse ZFS parameter E is close to zero and the uniaxial anisotropy parametrized by D is increased.[7] The pseudo tetrahedral geometry around the Co(II) ion is useful in this situation because it allows for improved spin-orbit coupling between the ground and excited states. Sulfur functionalized ligands are advantageous for anchoring the magnetic cluster on the gold surface.[28] Many Co(II) SIMs with N_2O_2 donor-sets have been described in recent years, and they are known to exhibit slow relaxation of magnetization at zero field or applied dc field.[24,25,29] The relative arrangements of d-orbitals of four coordinate Co(II) ions can change with the distortion of the coordination geometry. All important parameters related to slow relaxation of magnetization of previously reported Co(II)-complexes with a pseudo tetrahedral coordination geometry are listed in Table S1. Here, we report for a new Co(II) based SIM [(LS)$_2$Co(**1**)] with the Schiff base ligand (HLS) and a NO donor-set the results of comprehensive structural and chemical analysis. Based on this information multi configurational SA-CASSCF/NEVPT2 theoretical calculations have been performed that are compared with the results from magnetic model fitting to experimental dc magnetization data. Furthermore, the dynamic magnetic properties are investigated by ac susceptibility for a broad variety of external dc magnetic fields and temperatures. In this study a competitive axial/transverse
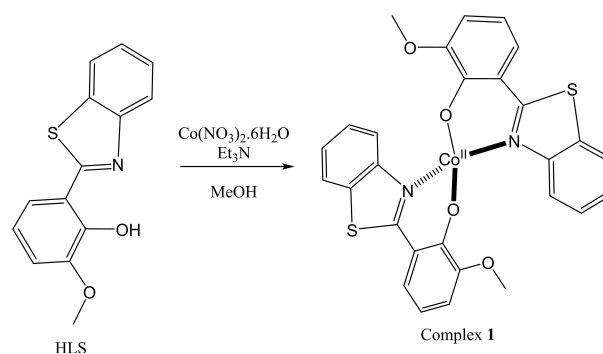
relaxation has been explored/studied along with different mechanism of reorientation of spin/magnetization under a wide range of applied dc magnetic fields. The fitting of the ac data produces a deeper insight of a complex interplay of mechanism of magnetic relaxation.

Results and Discussion

Synthesis. Schiff base ligand HLS (stands for neutral ligand with LS referring to the deprotonated mono anionic ligand) was prepared by condensation reaction between o-vanillin and 2-aminothiophenol (1.56 mL) in 1:1 molar ratio (Scheme S1) under aerobic condition.[30] The product was recrystallized from MeOH. Additionally, X-ray single crystal structure was determined for HLS ligand (Figure S1, Table S2 and Table S3). A 1:1 molar mixture of Co(NO$_3$)$_2$·6H$_2$O and HLS reacted in the presence of an equivalent amount of triethylamine base (Scheme 1). After a few other reaction steps as described in detail in the experimental part, dark blocks single crystals finally formed via slow evaporation of the filtrate in air at room temperature as complex **1** (Figure 1) with a yield of 15%.

Single-crystal X-ray analysis. Complex **1** crystallizes from MeOH in the orthorhombic space group *Pbcn* (Table S2). Except for the Co, all atoms occupy the general 8d Wyckoff site. The Co(1) possesses a distorted pseudo-tetrahedral coordination geometry with a O$_2$N$_2$ donor set sitting on the 4c Wyckoff position with '.2.' site symmetry. The Co—O and Co—N bond lengths are 1.906(3) and 1.999(4) Å, respectively (see also Table S4 for list of bond lengths and bond angles). These bond parameters are comparable to those of previously reported Co-complexes. The packing diagrams of complex **1** are shown in Figure S2 and Figure S3. There are π-stacking (3.5 Å) interactions between the molecules (Figure S2).

Bulk purity was confirmed by elemental analysis of pure crystals of complex **1** (Table S5). This complex is stable in solution as confirmed by the HRESI-MS spectrum (Figure S4) that returns a mass matching with complex **1** as $m/z = $ [M + Na]$^+$ ion: [M$=$C$_{28}$H$_{20}$CoN$_2$O$_4$S$_2$]. Elemental (C, H, N) analysis for C$_{28}$H$_{20}$CoN$_2$O$_4$S$_2$ (calcd.): C 58.78 (58.84), H 3.57 (3.53), N 4.84 (4.90). Complex **1** has further been studied by temperature dependent ^{1}H NMR in two non-coordinating solvents: polar
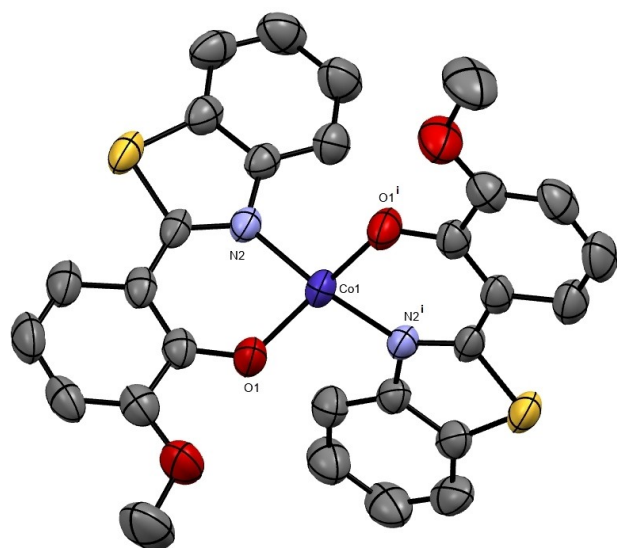

Scheme 1. Synthesis of complex **1**.

EurJIC
European Journal of Inorganic Chemistry

Research Article
doi.org/10.1002/ejic.202200774

**Chemistry
Europe**
European Chemical
Societies Publishing

Figure 1. ORTEP drawing of complex [(LS)$_2$Co(II)] (**1**) with thermal ellipsoid shown at 50% probability level. (i) $-x+1$, y, $-z+1/2$.

CDCl$_3$ (Figure S5) and non-polar C$_6$D$_6$ (Figure S6). The temperature dependent chemical shift (δ) is opposite for both solvents what might be due to the different extent of ring currents that are produced by the solvent-solute dipolar interactions (magnetic moments of the nucleus and unpaired electrons).[31]

IR spectroscopy. In the IR spectra of complex **1** (Figure S7), the stretching vibration of the free ligands (ν_{OH}) 3430–3464 cm^{-1} is not observed, suggesting deprotonation of the hydroxyl group and formation of metal-oxygen bonds. A Methyl group attached to a benzene ring exhibits two IR bands: one is C–O and another is phenyl-O. The C–O stretching band would be visible in the range 1045–1049 cm^{-1}. However, the observed 1245–1248 cm^{-1} band is due to the symmetrical phenyl C–C bond stretching. A close look at the low frequency region of the spectra reveals the presence of medium intensity bands in the region of 300–600 cm^{-1} due to ν_{M-N} and ν_{M-O}. The intensity of the bands in the region 700–800 cm^{-1} is due to ν_{C-H} and ν_{C-S} stretching. The strong bands appearing in the region 1600–1647 cm^{-1} were assigned to $\nu_{C=N}$ stretching. The shifted frequency compared with that of corresponding ligands HLS indicate the coordination by nitrogen of the azomethine $\nu_{C=N}$ group.

UV-VIS. UV-VIS spectra of complex **1** in different solvents show absorption bands around 300 and 385 nm. In THF an additional band appears at 535 nm due to deviation from tetrahedral coordination geometry towards a square planar geometry (Figure S8). The color change of a Co(II)-complex has been previously reported due to significant structural distortions.[32] TD-DFT calculations were performed to assign the electronic transitions in **1** (Figure S9) using the optimized geometry of **1** although it cannot account for the effect of structural distortion due to the nature of the solvent-interaction other than considering the dipole-dipole interactions between **1** and the solvent molecules. The dark blocks of **1** produce dark

red solution in THF while they show dark green color in CHCl$_3$ (Figure S10). The intensity of the red THF solution decreases with time leading to a light-yellow colored solution (Figure S11). This could be due to the rotation of the LS ligand around the Co-center and/or structural distortions to attend an equilibrium in THF. A photochromic tetrahedral Co(II) SIM was reported before.[25]

Cyclic voltammogram (CV). The cyclic voltammograms of Co(II) complex **1** shown in Figure S12 were recorded in THF solvent at room temperature and under N$_2$ gas atmosphere. Complex **1** showed one electron irreversible process at potential $P_{1/2} = (P_{oxidation} + P_{reduction})/2 = 0.15$ V corresponding to an oxidation. The CV suggests that complex **1** can irreversibly undergo (at the scan rate of 25 mV s^{-1}) one electron oxidation to form a possible Co(III)-analogue (**1**$^+$) of complex **1**. A dark blue colored crystalline powder was obtained when complex **1** was oxidized by (NH$_4$)$_2$Ce^{IV}(NO$_3$)$_6$ ($P_{1/2} = 1.61$ V).

Theoretical calculation. From the effective Hamiltonian approach (Eq. S1) the g-values $g_x = 2.12$, $g_y = 2.12$, $g_z = 2.52$ and $g_{iso} = 2.25$ were obtained for complex **1** (see also Figure 2 and Supporting Information, Table S6 for Kramer Pair components). The D-tensor components (Eq. S2) are listed in Table S7 with the resulting axial and transverse zero-field splitting (ZFS) parameters $D = -35.41$ cm^{-1} and $E = -0.62$ cm^{-1}, respectively, and the ratio $E/D = 0.017$. For $E \neq 0$ the energy between the ground and the first excited Kramer pair is given by $\Delta E = 2\sqrt{D^2 + 3E^2} = 70.85$ cm^{-1}.

The ground Kramer pair $|\varphi_1\rangle$ with mainly $|\pm 3/2\rangle$ contribution is predominantly axial with $g_z = 7.55$ and g_x, $g_y = 0.11$ and the first excited Kramer pair $|\varphi_2\rangle$ with mainly $|\pm 1/2\rangle$ contribution has a rhombic character with $g_x = 2.55$, $g_y = 4.12$, $g_z = 4.35$ (see Table S8 for description of Kramer pair wave functions). The angle between the g_z component of the ground
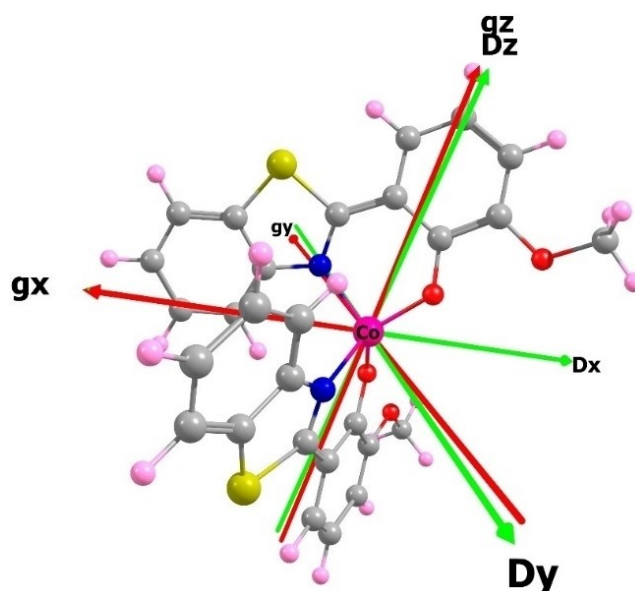

Figure 2. The orientation of the g-tensor and D-tensor principal components for the ground state of complex **1** in the molecular frame. The red, blue, grey, light pink and dark pink atoms are O, N, C, H and Co, respectively.

EurJIC
European Journal of Inorganic Chemistry

Research Article
doi.org/10.1002/ejic.202200774

Chemistry Europe
European Chemical Societies Publishing

Kramer pair and the first excited Kramer pair is 92.13°. Since $E \neq 0$, there is quantum mechanically mixing of the ground Kramer pair with the excited Kramer pair.

The D value given above was obtained from effective Hamiltonian approach. For further qualitative understanding of which kind of electronic transitions and splitting of d-orbitals are involved, the second order spin-orbit coupling (SOC) contribution to D value is further determined by *ab initio* ligand field theory approach. All the roots arising from quartet and doublet multiplicity were included to have effective spin-orbital coupling between ground and excited states. The ground and excited states of the Co(II) ion here are coupled by the orbital angular momentum operator whose coupling strength is determined by the Λ-tensor and gives the contribution to the D value (see Equation S3).[33] The degenerate energy states will not contribute to D, whereas the near degenerate states have large contributions. When the electronic transition occurs between the energy states corresponding to the same $|m_L|$ values, it contributes negatively to the overall D value and if the electronic transition occurs between the energy states corresponding to different $|m_L|$ values, it contributes positive to the overall D value. Since the CASSCF is a multi-configurational respectively multi-determinant method, the ground state of the complex cannot be represented by a single determinant. It has significant contribution from other electronic configurations as outlined in Table S9. For the ground state the electronic transition mainly occurs from d_{xz} to d_{yz} with same $|m_L|$ value and negative contribution to D, whereas the second excited state indicates a transition from d_{x2-y2} to d_{yz} with different $|m_L|$ value and positive contribution to D value.[33] Similarly, the contributions from the third and fourth transitions are positive and negative to overall D value (see Table S10). As the energy difference between the states becomes large, the contribution to the D value becomes small. Especially for understanding the dynamic magnetic properties of the complex **1**, the calculated magnetic transversal magnetic moments from *ab initio* method are of great importance as illustrated in Figure 3. If E would be zero a transition from $|-3/2\rangle$ to $|+3/2\rangle$ would only be

possible via a transition to $|-1/2\rangle$ and $|+1/2\rangle$. Since the $|\pm 1/2\rangle$ states then would represent the excited Kramer pair the energy barrier would need to be overcome to go from $|-3/2\rangle$ to $|+3/2\rangle$ by thermal activation. This would result in a pronounced slow magnetic relaxation and a very stable $|\pm 3/2\rangle$ spin state conservation over time as desired for applications. Since for complex **1** $E \neq 0$ there are non-zero transition probabilities for a direct transition from $|-\varphi_1\rangle$ to $|+\varphi_1\rangle$ but also from the excited states $|\pm\varphi_2\rangle$ to $|\pm\varphi_1\rangle$ that can be classified as direct and thermal assisted QTM, respectively. These relaxation pathways are opposing slow magnetic relaxation as further investigated experimentally by ac magnetic susceptibility measurements presented below. These competitive axial and in-plane relaxation processes may have further slowed down the overall magnetic relaxation. It further may influence the relaxation mechanism which can be studied under applied dc magnetic field. AILFT calculations (Figure 4 and Figure S13) were carried out to qualitatively study the electronic transition occurring within this Co(II)-complex and correlate with its contribution to ZFS-tensor.

Dc magnetic properties. A Curie-Weiss fit according to Equation (S4) to the experimental inverse susceptibility data of complex **1** from 50 to 250 K (Figure S14) returns a molar Curie constant of $C_{mol} = 2.698(4)$ cm^3 K mol^{-1} and a Weiss constant $\theta = -3.61(2)$ K. From the molar Curie constant an effective paramagnetic moment of $\mu_{eff} = 4.65(1)$ μ_B can be calculated. Co(II), as a free ion, has [Ar] 3d^7 electronic configuration with three unpaired electrons with a total spin quantum number $S = ^3/_2$ for
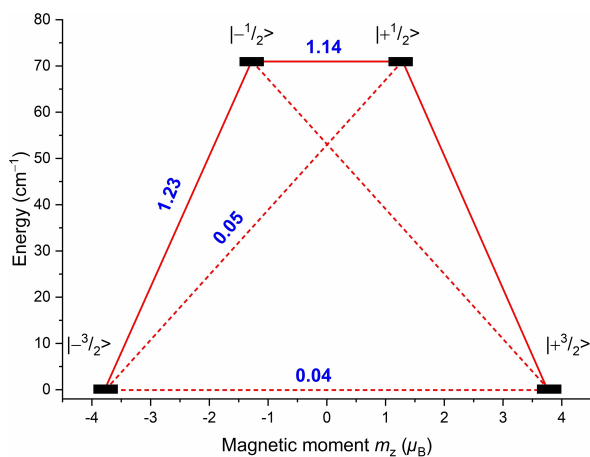
Figure 3. *Ab initio* calculated blocking barrier for complex **1** with magnetic transition moments (blue) and corresponding pathways (red lines).
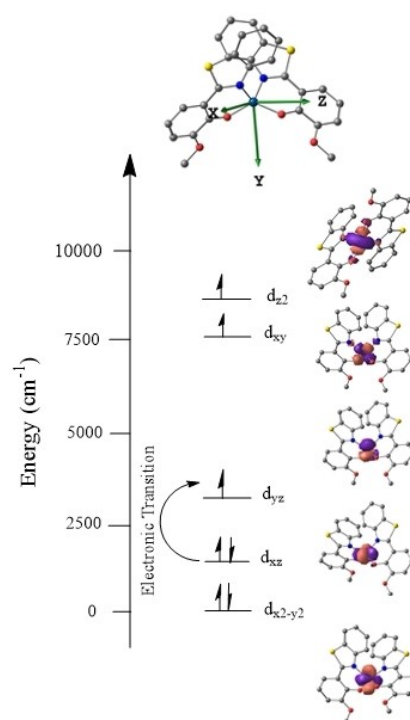
Figure 4. *D*-orbital splitting diagram computed by AILFT on the SA-CASSCF +NEVPT2-SC level of theory. The electronic transition from d_{xz} to d_{yz} is shown and is within same $|m_L|$ value. The molecule with reference axes frame is shown at the top and the hydrogens are omitted for clarity purpose.

EurJIC
European Journal of Inorganic Chemistry

Research Article
doi.org/10.1002/ejic.202200774

Chemistry
Europe
European Chemical
Societies Publishing

a high spin configuration, independently from the specific crystal field symmetry. Obviously, there is a considerable contribution from orbital angular momentum to the spin-only paramagnetic moment of 3.87 μ_B for $S = ^3/_2$. In full analogy to the effective spin Hamiltonian approach presented in the theoretical calculationssection above, 'model ZFS' returns the refined parameters $D = -37.42$ cm^{-1} and $E = -0.61$ cm^{-1} with $E/D = 0.0163$ that describe the experimental susceptibility vs. temperature and magnetic moment vs. field data to sufficient agreement (see Figure 5, Figure S15 and Table S11). These values are very close to those obtained from the theoretical *ab initio* calculations and, as illustrated in Figure S16, the χT vs. temperature and magnetic moment vs. field curves as calculated from theoretically determined D, E and g values are also close to those experimentally measured. The refined g values deviate substantially from the calculated ones. In most cases, magnetometry data is insufficient to reliably determine anisotropic g values and more sophisticated spectroscopic methods have to be utilized. Consequently, only isotropic g values are often refined to magnetometry data sets in order to avoid over-parametrization. However, since for complex **1** isotropic g value fits resulted in considerably worse fits, the anisotropic values
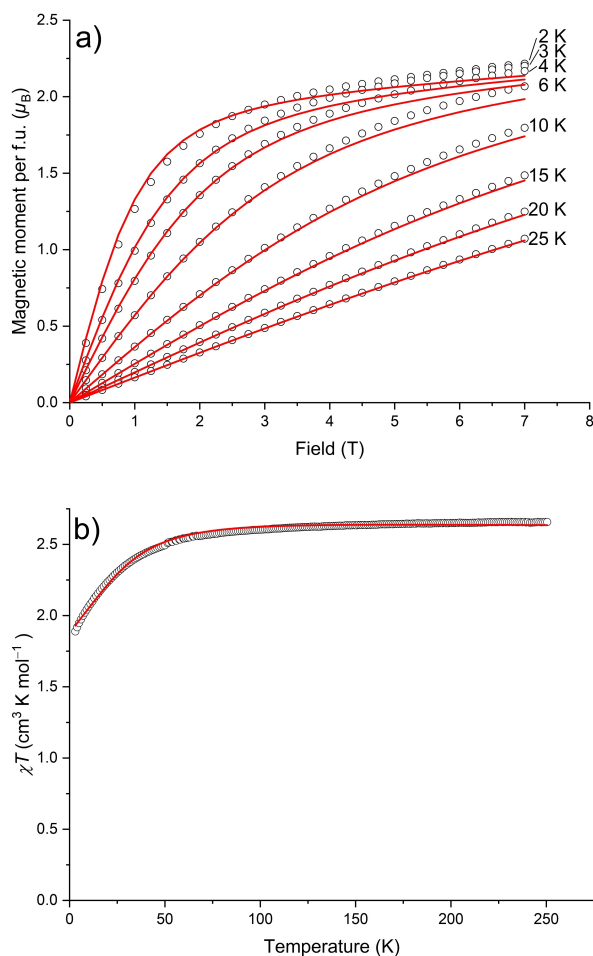
are still given here. Despite the orbital contribution of about 0.78 μ_B per Co ion to the spin-only value, the magnetic system of complex **1** can still be described adequately by a phenomenological spin Hamiltonian approach on the basis of the spin only value of $S = ^3/_2$, i.e. the orbital contribution only enters as a second order perturbation as outlined above. If a first order orbital momentum of considerable size would first couple to the spin angular momentum, a low energy $J = ^1/_2$ doublet, an intermedium energy $J = ^3/_2$ quartet and a high energy sextet $J = ^5/_2$ would have formed. This represents a hypothetical Co^{2+} with d^7 electronic configuration in an octahedral crystal field with a triplet $^4T_1$ ground state that allows for contribution for orbital momentum (no quenching). These J-multiplets might then further be split according to the axial and transverse crystal field splitting terms due to a lowered site symmetry. A fit according to this alternative model that makes use of the so-called $T \equiv P$ isomorphism[34] (T stands for triplet and P for p orbital) even exhibits a better agreement with the experimental data, but the remarkably large absolute values of the refined crystal field parameters ($B_2^0 = -222(1)$ cm^{-1} and $B_2^2 = -125.5(5)$ cm^{-1}) and, even more importantly, their ratio indicate that this is not an adequate description for the magnetic properties of complex **1**. By the large values of the crystal field parameters the J-multiplets are rearranged in such a strong way that the important low-lying energy states can equally be represented by a simple $S = J = ^3/_2$ system again as already used for 'model ZFS'. Therefore, this alternative approach was discarded and is not shown in detail here.

Ac magnetic properties. Complex **1** does not display slow relaxation of magnetization under zero dc field as confirmed by frequency dependent AC susceptibility measurements from 1.8 K to 8 K and from 10 Hz up to 10 kHz. At 0.01 T, a slow magnetic relaxation manifests as a maximum in the imaginary $\chi''(\omega)$ ac susceptibility signal (see Figure 6 for exemplary χ' (a) and χ'' (b) vs. frequency plots measured at 0.2 T and Figure S17 for a complete listing for all fields). Relaxation times τ together with their uncertainty values were obtained from the ac susceptibility measurements according to Equation S6 in a temperature range from 1.8 to 8 K for 14 different dc fields ranging from 0.01 to 1 T. The Cole-Cole plots (Figure S17) for different temperatures deviate from a semi-circular shape and are described by a generalized Debye model that considers a distribution of relaxation times by the parameter α that is ranging from 0.02 to 0.4. It should be emphasized that adequately considering the uncertainties of the extracted relaxation times is mandatory to finally obtain correct uncertainties for the parameters describing the relaxation processes.[35] From the double logarithmic plots of the inverse relaxation times τ^{-1} vs. temperature (see Figure 6c for exemplary plot at 0.2 T with individual fit contributions, Figure 7a and b for summary plots for all temperatures, and Figure S18 and S19 in the Supporting Information for a complete listing of the individual fits) two regimes with dominance of different types of relaxation mechanisms can be inferred according to following Equation (1) as taken in a modified form from literature[35]:
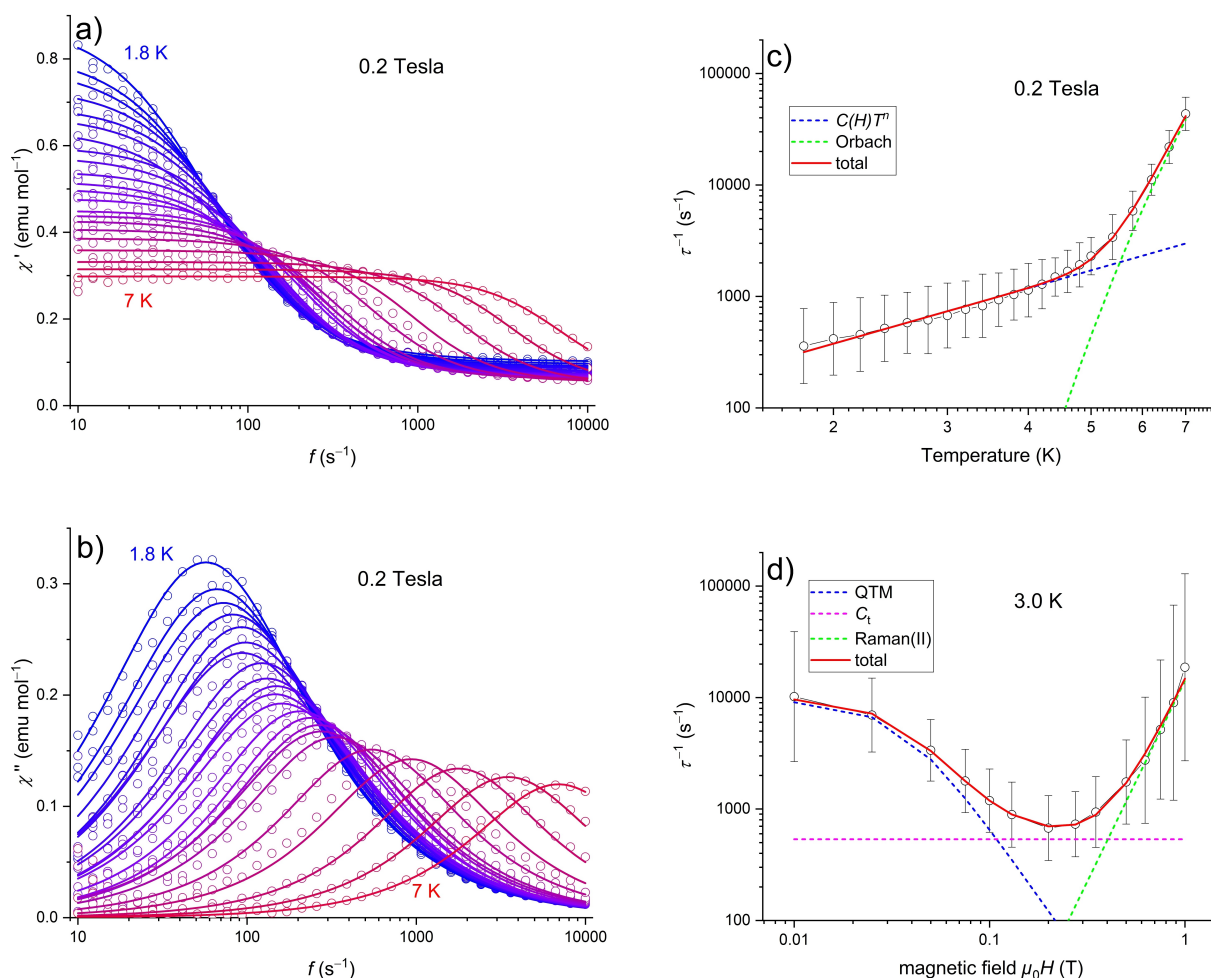

Figure 5. Experimental (black circles) a) magnetization vs. field and b) $\chi'T$ vs. temperature plots of complex **1** together with fit curves (red) according to magnetic 'model ZFC'.

EurJIC
European Journal of Inorganic Chemistry

Research Article
doi.org/10.1002/ejic.202200774

Chemistry Europe
European Chemical Societies Publishing

Figure 6. Exemplary plot (for 0.2 T) of experimental χ' (a) and χ'' (b) vs. excitation frequency f (open symbols) together with fits according to Equation (S6) to extract the relaxation rates τ (from 1.8 K to 5 K with 0.2 K increment and from 5.4 to 7 K with 0.4 K increment). Exemplary plots of inverse relaxation rates τ^{-1} vs. temperature at 0.2 T (c) and vs. field at 3.0 K (d) together with fits according to Equation (1) and Equation (2), respectively. See Figures S17, S19 and S21 in Supporting Information for a complete listing of these figures for all temperatures and fields.

$$\tau^{-1}(T) = C(H)T^{n(H)} + \tau_0^{-1}(H)\exp(-U_{\text{eff}}/T), \qquad (1)$$

where the first term covers relaxation processes commonly introduced as a sum of a Raman $C_R T^n$, a direct $A(H)T$ and a temperature independent quantum tunneling term τ_{QTM}^{-1}. An argument for this reduction to a single $C(H)T^{n(H)}$-term here is given in the end of this section. $C(H)$ can be considered as a zero-temperature extrapolation of the relaxation times as a function of magnetic field and will be discussed below in more detail when the relaxation times vs. magnetic fields plots are presented. In the low temperature regime up to about 5 K, the field dependent relaxation mechanism according to $C(H)T^{n(H)}$ is dominating (Figure 7a). In zero field, complex **1** does not show intrinsic relaxation due to the non-zero transverse ZFS contribution E that allows for magnetic reversal via direct tunneling between the ground state Kramer pair $|\pm \varphi_1\rangle$, i.e. there is no energy transfer between the spin and lattice involved. By introducing a dc magnetic field, the corresponding Zeeman energy that is created/annihilated by magnetic reversal needs to be compensated by the lattice. According to the calculations

presented in Table S12 the experimentally determined magnetic moment of complex **1** would approximately exhibit a Zeeman energy of approximately $1.81\ \text{cm}^{-1}$ at 1 T for the hypothetical free ion case. From 0.01 T to about 0.2 T, $C(H)$ is decreasing continuously while the temperature exponent $n(H)$ approximately is constant at ~ 2 (Figure 8). This T^2 dependence of inverse relaxation times on temperature points to a direct single phonon spin-lattice relaxation where the Zeeman energy of magnetic reversal by tunneling is compensated by corresponding annihilation/creation of a single phonon. The number of available phonons of a certain energy increases roughly with a linear temperature dependence and a T^2 dependence is then commonly observed when the heat transfer within the lattice is a limiting factor ('bottleneck'). The lowest relaxation rate of 2.79(2) ms (corresponds to inverse relaxation rate of 358(3) s^{-1}) is measured at 1.8 K and 0.2 T for complex **1**. When the field is increased above 0.2 T, the average value of the temperature exponent $n(H)$ slightly decreases and approaches ~ 1, i.e. a direct relaxation mechanism is still supposed to be present but without the heat transfer within the lattice being the limiting

EurJIC
European Journal of Inorganic Chemistry

Research Article
doi.org/10.1002/ejic.202200774

Chemistry
Europe
European Chemical
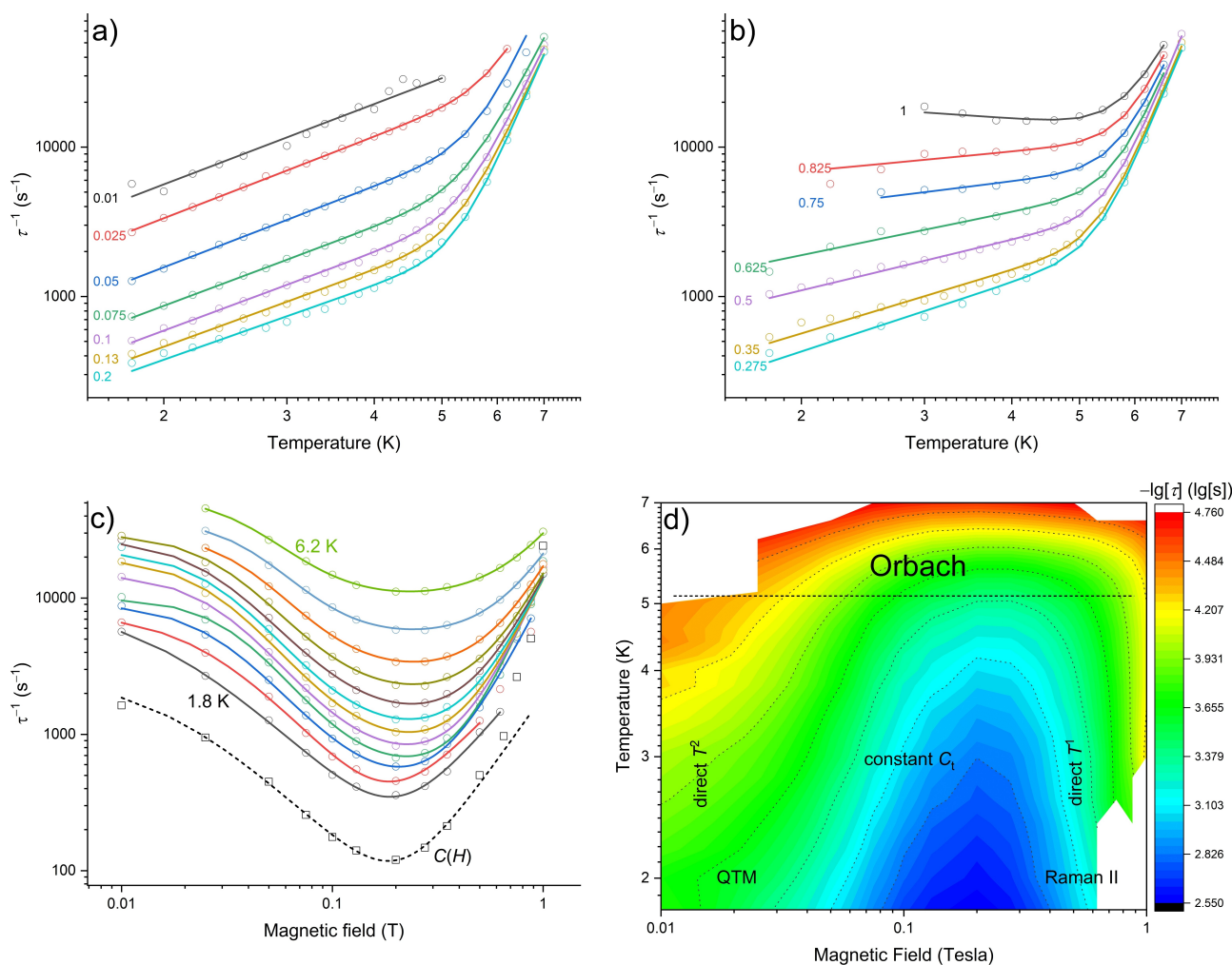Societies Publishing

Figure 7. Experimental inverse relaxation times (open symbols) as a function of temperature for magnetic dc fields from a) 0.01 to 0.2 T and b) from 0.275 to 1 T together with fits (lines) according to Equation (1). c) Experimental inverse relaxation times as a function of magnetic dc field for various temperatures together with fits according to Equation (2). d) contour plot of experimental inverse relaxation times as a function of both, magnetic field and temperature, with dominant relaxation processes as determined by Equation (1) inserted with vertical text alignment and those as determined by Equation (2) inserted with horizontal text alignment.

factor anymore. However, large standard deviations are present and a trend of evolution of $n(H)$ cannot unambiguously be claimed, especially concerning the high field region. For temperatures above 5 K, an Orbach relaxation process (second term in Equation (1)) is dominating the relaxation times as a function of temperature. The refined Orbach energy barrier is about ≈ 80 K (equals 55.6 cm^{-1}) and the attempt frequency τ_0^{-1} is approximately 10^{-10} s^{-1}, both without any observable dependence on dc field but comparably large standard deviations (see Figure S20). Here the magnetization reversal occurs via an excitation from the ground state Kramer pair with mainly $|\pm 3/2\rangle$ contributions to the excited Kramer pair with mainly $|\pm 1/2\rangle$ contributions. The Orbach energy barrier U_{eff}, as determined from the ac susceptibility measurements, is of comparable size as the energy difference $\Delta E = 70.85$ cm^{-1} between the Kramer ground and first excited state calculated from the ZFS parameters D and E (from *ab initio* calculations). During the magnetic reversal via the thermally activated energy

barrier, a phonon of matching energy is created and annihilated (two phonon process) for the Orbach process. As can exemplarily be inferred from Figure 6c for 0.2 T, an adequate fit to the plots of inverse relaxation rate vs. temperature can be obtained by a single T^n-term with n ranging between 1 and 2 for all fields, i.e. by a kind of variable direct term (T^1) that also can cover 'bottleneck' effects (T^2). Adequate here means that, accounting for the errors associated with the data points, an additional Raman term $C_R T^n$ (with n typically in the range from 7 to 9) to the direct term would lead to an over-parametrization. In the transition region from about 5 to 6 K where the slope changes tremendously from a direct (with potential 'bottleneck') to an Orbach relaxation process such a term with n ranging from 7 to 9 could be added in principal. But it would only have a minor contribution to the total fit by a sufficiently low valued C_R pre factor (that would not contain a physical meaning).
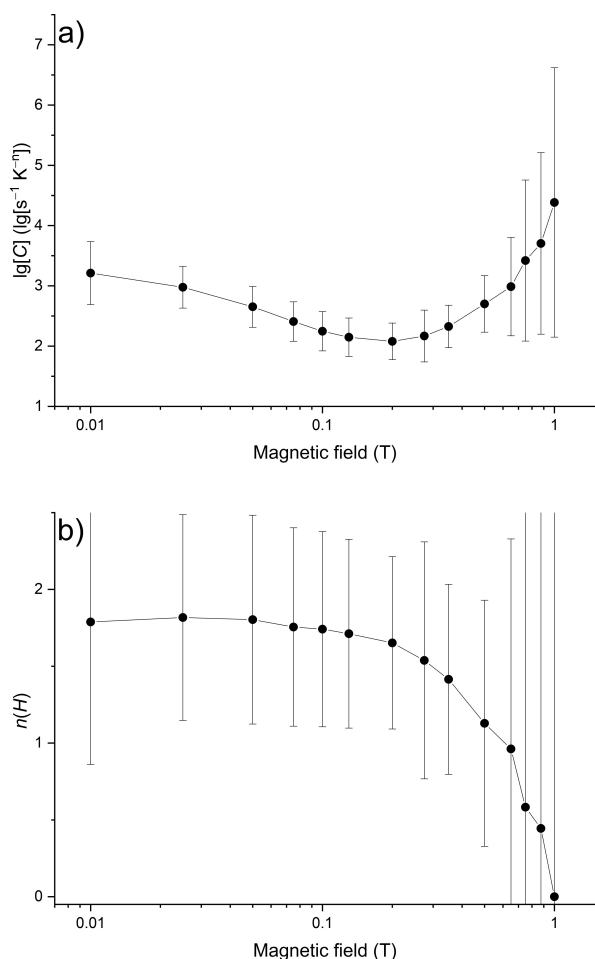
EurJIC
European Journal of Inorganic Chemistry

Research Article
doi.org/10.1002/ejic.202200774

**Chemistry
Europe**
European Chemical
Societies Publishing

Figure 8. Obtained evolution of a) $C(H)$ and b) $n(H)$ parameters for complex **1** as a function of magnetic field.

Inverse relaxation times τ^{-1} vs. magnetic field curves for various temperatures are exemplarily shown for 3 K in Figure 6d with individual fit contributions and for all temperature in summary in Figure 7c (see Figure S21 for a listing of all individual fits). These curves were fitted according to Equation (2) as taken in a modified form from literature[35]:

$$\tau^{-1}(H) = \frac{\tau_{\text{QTM}}^{-1}(T)}{1 + \tau_{\text{QTM}}^{-1}(H, T) \cdot H^{p(T)}} + C_{\text{II}}(T)H^{m(T)} + C_{\text{t}}(T), \quad (2)$$

with a so called quantum tunneling term parametrized by $\tau_{\text{QTM}}^{-1}(T)$, $\tau_{\text{QTM}}^{-1}(H, T)$ and $H^{p(T)}$, a second-order Raman(II) term $C_{\text{II}}(T)H^{m(T)}$ and a field independent term $C_{\text{t}}(T)$. In general, the quantum tunneling and the Raman(II) term are explaining the evolution of relaxation rates vs. field predominantly in the low and in the high field region, respectively (Figure 6d and S21). The $C(H)$term as introduced above represents a kind of zero temperature extrapolation of the inverse relaxation times as a function of magnetic field. The magnetic field exponent $p(T)$ of the quantum tunneling term starts at around 2.0 for low temperatures (Figure S22). Approximately above 2.5 K, the constant term $C_{\text{t}}(T)$ abruptly comes into play and keeps

increasing with increasing temperature. Simultaneously, with the sudden increase of the $C_{\text{t}}(T)$ parameter a significant change of the $C_{\text{II}}(T)$ and $m(T)$ parameter (from $m(T) = 2$ to approximately $m(T) = 4$) of the Raman(II) process is at least indicated but remains ambiguous due to the large standard deviations of the parameters. The contour plot presented in Figure 7d serves as base to discuss the inverse relaxation times of complex **1** as a function of both, field and temperature. At temperatures above 5 K, magnetization reversal via the excited states with mainly $|\pm 1/2\rangle$ contribution that requires to overcome the energy barrier by thermal excitation gets feasible. This spin-lattice relaxation is characterized by a two-phonon annihilation/creation process (Orbach). On the other side, at very low temperature, where thermal excitement over this energy barrier can be neglected, quantum tunneling mechanism (QTM) is the prevailing mechanism of magnetic reversal. For non-zero fields the Zeeman energy difference that is related to the magnetic reversal by QTM is compensated by a single phonon ('direct') creation or annihilation, respectively. At a given temperature with a certain phonon population, increase of the field and thereby the energy difference reduces the inverse relaxation times as convincingly shown by the $C(H)$ term at the low field region. Since the number of phonons with a certain energy approximately follows a linear temperature dependence, the inverse relaxation times would increase linearly with temperature in the same region if not limiting heat transfer effects would finally lead to a T^2 temperature dependence. Under applied dc field of around 0.2 T, the inverse relaxation times have a minimum and a further increase of the field results in higher inverse relaxation times again. At these higher fields, the lattice energy difference of magnetic reversal is indicated to be compensated by a second-order Raman(II) process (see Equation (2)) with creation and annihilation of two phonons via a virtual excited state. It should be noted, that the temperature exponent $n(H)$ for the same very low temperature/high field region is still refined to ~1.0 in this region as far as it can be determined considering the large standard deviations. 'Normally', for a Raman relaxation process according to a term $C(H)T^{n(H)}$, exponents n of about 9 (Kramer system) or about 7 (non-Kramer systems) are characteristic (values as small as ~5 were only described theoretically at high Debye limit[36]). Therefore, a certain disagreement has to be attested here, since what is called a second-order Raman(II) process for the low temperature/high field region according to the field dependent description, still has very low values $n(H)$ of about ~1 as inferred according to the temperature dependent description that therefore cannot be related to Raman relaxation processes. Since the Orbach process dominates at temperatures greater than 5 K with negligible dependence on the magnetic field, a field-independent term $C_{\text{t}}(T)$ contributes more and more. Table S1 lists for a variety of Co-complexes with (pseudo) tetrahedral and octahedral coordination the experimentally determined relaxation parameters according to an Orbach, a direct, a Raman and a QTM process. Complex **1**, as most of the listed complexes, exhibits an Orbach process with comparable values for attempt frequency and energy barrier and further a 'direct' term also with a comparable value for relaxation

EurJIC
European Journal of Inorganic Chemistry

Research Article
doi.org/10.1002/ejic.202200774

**Chemistry
Europe**
European Chemical
Societies Publishing

frequency. As outlined above, Equation (1) does not include an explicit Raman term due to over-parametrization.

Conclusion

A Co(II)-complex with a N_2O_2 donor-set has been theoretically studied by multi configurational SA-CASSCF/NEVPT2 method predicting that the Co(II) center of this complex has a total spin $S = 3/2$ that experiences a mixture of uniaxial ($D = -35.41$ cm^{-1}) and transverse ($E = -0.62$ cm^{-1}) zero field splitting. These values are in good agreement with refined parameters $D = -37.42$ cm^{-1} and $E = -0.61$ cm^{-1} that reproduce the experimental temperature and field scans most adequately. Due to the transverse ligand field contribution to the ZFS, there is a considerable mixture between the Kramer ground state that mainly consists of $|\pm 3/2\rangle$ spin states and the first excited Kramer state that mainly consists of $|\pm 1/2\rangle$ states. As a consequence, magnetic reversal from $|-3/2\rangle$ to $|+3/2\rangle$ is not restricted to occur only via an energy barrier ΔE, but can be surpassed also by QTM and complex **1** does not exhibit slow relaxation (within the given experimental techniques) in zero dc magnetic field. By applying a dc magnetic field, the magnetic reversal by quantum tunneling relates to a Zeeman energy difference that has to be compensated by the lattice. At low temperature and low field, the spin-lattice relaxation occurs via a 'direct' one phonon process that is limited by heat transfer and therefore shows a T^2 temperature dependence. At higher fields (above ~ 0.2 T) the heat transfer is no longer a limiting factor and a 'direct' process with a linear temperature dependence can be observed. In general, all extracted parameters from the ac susceptibility measurements exhibit quite large standard deviations and trends that are suggested by the average values should be considered critically. At higher temperature greater than 5 K, the magnetic reversal via the energy barrier ΔE, i.e. via the excited states with mainly $|\pm 1/2\rangle$ contribution, gets feasible. Here, the spin-lattice relaxation can be described by an Orbach process with $U_{eff} \approx 80$ K (equals 55.6 cm^{-1}) what is quite close to the energy barrier $\Delta E = 70.85$ cm^{-1} as determined theoretically from the ZFS parameters. In a combined presentation of the inverse relaxation times as a function of both, temperature and field, an inconsistency regarding the labeling of the relaxation processes became apparent: what is labelled as a second-order Raman(II) process for the high field/low temperature region in the field dependent description of the relaxation rates, still appears as a direct process with linear or T^2 temperature dependence in the temperature dependent description. 'Normally', a Raman relaxation process is considered to be present for temperature exponents that are much higher (n approximately between 7 and 9). In summary, due to the given coordination of the Co(II)-complex with a N_2O_2 donor-set, the transverse component of the ligand field prevents the complex from exhibiting intrinsic slow magnetic relaxation at elevated temperatures.

Experimental Section

Synthesis

Synthesis of ligand HLS: The o-vanillin (2739.4 mg, 18 mmol) is dissolved in MeOH (25 mL) and 2-aminothiophenol (1.56 mL, 15 mmol) added slowly by a syringe (1:1 molar reaction). The solution was refluxed with continuously stirring for 1 hour. On cooling, the yellowish orange crystalline product of HLS was separated out, washed with cold MeOH and dried. The product was recrystallized from MeOH. HLS stands neutral ligand and LS refers to deprotonated mono anionic ligand.

Synthesis of complex (LS)₂Co^{II} (1): A 1:1 molar mixture of Co(NO$_3$)$_2$·6H$_2$O (0.2 mmol, 58 mg) and HLS (0.2 mmol, 51 mg) was placed in a 100 mL conical flask and MeOH (25 mL) was added. The reaction mixture was stirred for five minutes to get a clear yellow-orange solution and then triethylamine (Et$_3$N) (0.2 mmol, 20 mg) was added at room temperature. The color of the solution slowly turned to pale pinkish yellow from dark yellow. The stirring was continued for further ten minutes to produce a crystalline greenish precipitate which was separated by filtration. The faint green colored filtrate was stored at room temperature in a dark place for two nights and then at normal place in the laboratory (in the presence of light). Dark blocks single crystals suitable for X-ray single crystal diffraction are formed via slow evaporation of the filtrate in air at room temperature. The yield is 15%. EPR active $g = 2.271$. A similar reaction with 1:2 molar ratio of Co(NO$_3$)$_2$·6H$_2$O and HLS in the presence of the calculated amount of a base (Et$_3$N) did not lead to the isolation of complex **1** instead led to the formation oily liquid.

Structure and Composition

Fourier-transform infrared spectroscopy (FTIR): FTIR spectrometer was used to record the infra-red (IR) spectra in the range 4000–400 cm^{-1} using pressed pellet sampling technique/KBr discs. A small amount of IR-grade KBr that covers an area of about 20 mm^2 to a depth of 1 mm was placed in mortars. A small amount of powdered sample was mixed with KBr and grinding until they are uniformly distributed throughout the KBr and transfer some of the mixture to the pellet making die. Finally, the pellet was made and the FTIR spectra were obtained.

Single-crystal x-ray analysis: Single crystal x-ray data were collected on a Bruker Axs Kappa Apex2 CCD diffractometer with graphite mono chromated Mo-K_α ($\lambda = 0.71073$ Å) radiation at 100 K. The data was integrated using SAINT PLUS[37] and absorption correction have been carried out using multi-scan absorption correction method (SADABS).[38] The structure was solved by direct method (SHELXS-97) and refined using SHELXL-2018/3 program and WinGX v1.70.01[39] programs packages. All non-hydrogen atoms were refined anisotropically. The crystals of complexes HLS and complex **1** were grown from concentrated MeOH solutions via slow evaporation of methanol. The per-fluorinated oil (average molecular weight is 3300 g/mol) which was purchased from Sigma Aldrich, used for single crystal mounting. The average data collection time was 8 h for a single crystal under flow of argon gas at 100 K.

Deposition Numbers 2167848 (for **1**), 2167936 (for HLS ligand) contain the supplementary crystallographic data for this paper. These data are provided free of charge by the joint Cambridge Crystallographic Data Centre and Fachinformationszentrum Karlsruhe Access Structures service.

Cyclic voltammetry (CV). CV experiments have been performed at a Metrohm-Autolab204 Potentiostat. All experiments have been

performed under argon atmosphere in deoxygenated and anhydrous THF solution of 0.1 M [n-Bu$_4$N]PF$_6$. The setup consisted of a glassy carbon (GC) working electrode (WE), a Pt wire as the counter electrode (CE) and an Ag wire as the reference electrode (RE). The recorded voltammograms have been referenced to the internal standard (fc)$_2$Fe$^+$/(fc)$_2$Fe, which was added after the measurements.

HRESI-MS. High resolution electrospray mass spectrometry measurements were conducted at a capillary temperature of 225 °C. Aliquots of the solution were injected into the device at a flow rate of 2.00 μL/min. The mass spectrometer used for the measurements was the Agilent Technologies 6545 Q-TOF LC/MS, and the data were collected in positive ion modes. The spectrometer was previously calibrated with the standard tune mix 75 to give a precision of ca. 2.0 ppm within the region of $m/z = 100$–3000. The capillary voltage was 2.5 kV, the tube lens voltage was 1.0 kV, and the skimmer voltage was 65 V.

CHN Analysis. Elemental analyses were performed on a Thermo scientific flash 2000 elemental analyzer under ambient conditions.

FTIR study. FTIR spectra were recorded for the solid samples sing KBr pellets on a Jasco FT/IR-4100 Spectrometer in the 400–4000 cm^{-1} range.

UV-VIS. UV-Visible Spectra of complex **1** were recorded on a Jaso V-650 Spectrophotometer in the range of 200–800 nm at room temperature.

Theoretical Calculations. All the quantum chemical (QC) calculations were performed by ORCA5 on the optimized geometry of the complex **1**.[40,41] The triple zeta valence basis set supplemented by two polarization functions (DEF2-TZVPP) was used for all atoms for all the calculations.[42] The geometry optimization was done with combined functional of Becke's exchange functional and Perdew's correlational functional (BP86) with Grimme's dispersion correction using D3BJ.[43] An auxiliary basis set was used in conjunction with the resolution of identity approximation to speed up the calculations.[44] The auxiliary basis set chosen for geometry optimization was -/JK type. Multi configurational method (CASSCF) was used to derive the Spin-Hamiltonian (SH) parameters and the magnetic characteristics of the complex **1**.[41] This calculation was performed over the optimized coordinates of **1**. Minimal active space of seven electrons in five 3d-orbitals CAS (7,5) was chosen based on Co (II) metal ion. All the roots arising from quartet and doublet multiplicities for 3d^7 configuration were taken into account i.e., 10 quartet roots from (^4F, ^4P) and 40 doublet roots (^2G, ^2P, ^2H, ^2D, ^2D, ^2F) (Table S13). With inclusion of all the roots with equal weight, the CASSCF calculation became state-averaged CASSCF. The dynamic correlation was included through strongly contracted N-electrons valence perturbation theory to second order (NEVPT2-SC).[45] The DKH formalism is included for taking the scalar relativistic effects into account.[46] For spin-orbit coupling, the mean-field approximation (SOMF) was utilized. The effective Hamiltonian approach was used to calculate the Spin-Hamiltonian parameters. SINGLE ANISO program was used to calculate the magnetic properties such as magnetic susceptibility at 0.1 T field, magnetization and ab-initio blocking barrier.[47] Ab-initio ligand field theory (AILFT) (Figure 4, Table S13, and Table S14) was utilized here to qualitatively study the electronic transition happening the complex and their contribution to ZFS-tensor.[41]

Magnetic Measurements. Dc magnetization was measured with a Physical Property Measurement System (PPMS DynaCool) from Quantum Design equipped with the vibrating sample magnetometry (VSM) option. A total sample mass of 12.7 mg of complex **1** (corresponds to $2.22211 \cdot 10^{-5}$ mol) was filled into a polypropylene capsule (QDS–P125E from Quantum Design) that was attached to the brass half tube sample holder for the dc magnetization

measurement and attached with some polyimid tape to a straw (Quantum Design) for the ac magnetization measurements.

Dc magnetization vs. temperature was measured at a field of 1000 Oe from 3 K to 50 K in settle mode and from 51 K to 250 K in sweep mode with 1 K/min heating rate. The temperature step size was 1 K with a signal averaging time of 10 seconds. The raw data has been corrected for temperature independent diamagnetic contribution stemming from the polypropylene capsule and from the atoms' closed shells as well as from the chemical bonds according to the incremental method[48] (see Table S15 for detailed listing and calculations). Magnetization vs. field was measured at 2, 3, 4, 6, 10, 15, 20 and 25 K up to 7 T with a field resolution of 2500 Oe (0.25 T) with a signal averaging time of 10 seconds and a two-fold redundancy per measuring point. Magnetic 'model ZFS' has been used for fitting of the dc magnetization data (please refer to Equation S 5, Supporting Information, for details of the corresponding Hamiltonian) using the PHI program package.[49] In full analogy to the *ab initio* calculations presented in this work, the magnetic Co(II) center is described by a constant total orbital quantum number $J = {}^3/_2$. Refinable parameters are the anisotropic effective g_{eff} values g_x, g_y and g_z restrained to be > 1.5, each, and the axial and transverse ZFS parameters D and E, respectively.

AC magnetization was measured with the ACMS-II option from 10 Hz to 10 kHz at 35 frequencies with log-distribution from 1.8 to 8 K (0.2 or 0.4 K temperature step depending on the temperature). The complete temperature scans were performed for 14 different magnetic dc fields ranging from 0.01 to 1 T. The ac excitation field was 5 Oe with an averaging time per measuring point of 10 seconds. For data evaluation of the ac susceptibility data set concerning the determination of the relaxation times as well as fitting of the relaxation models to the relaxation times vs. temperature and relaxation time vs. field data sets the program package CC-Fit2[35] was used. The complex-valued quantity of ac susceptibility $\chi(\omega)$ is composed by an in-phase or real component χ' and an out-of-phase or imaginary part χ'' according to the generalized Debye-model with a relaxation times distribution parameter α (Eq. S6).

Conflict of Interest

The authors declare no conflict of interest.

Data Availability Statement

The data that support the findings of this study are available in the supplementary material of this article.

[1] A. Caneschi, D. Gatteschi, R. Sessoli, A. L. Barra, L. C. Brunel, M. Guillot, *J. Am. Chem. Soc.* **1991**, *113*, 5873.
[2] R. Sessoli, D. Gatteschi, A. Caneschi, M. A. Novak, *Nature* **1993**, *365*, 141.

[3] M. Mannini, F. Pineider, C. Danieli, F. Totti, L. Sorace, P. Sainctavit, M.-A. Arrio, E. Otero, L. Joly, J. C. Cezar, A. Cornia, R. Sessoli, *Nature* **2010**, *468*, 417.

[4] L. Bogani, W. Wernsdorfer, *Nat. Mater.* **2008**, *7*, 179.

[5] M. N. Leuenberger, D. Loss, *Nature* **2001**, *410*, 789.

[6] Y.-Q. Zhai, Y.-F. Deng, Y.-Z. Zheng, *Dalton Trans.* **2018**, *47*, 8874.

[7] G. Peng, Y. Chen, B. Li, Y.-Q. Zhang, X.-M. Ren, *Dalton Trans.* **2020**, *49*, 5798.

[8] A. Zabala-Lekuona, J. M. Seco, E. Colacio, *Coord. Chem. Rev.* **2021**, *441*, 213984.

[9] F.-S. Guo, B. M. Day, Y.-C. Chen, M.-L. Tong, A. Mansikkamäki, R. A. Layfield, *Science* **2018**, *362*, 1400.

[10] C. J. Milios, R. E. P. Winpenny, *Cluster-Based Single-Molecule Magnets*, In: Gao, S. (eds) Molecular Nanomagnets and Related Phenomena. Structure and Bonding, Springer, Berlin, Heidelberg, **2014**, vol 164, https://doi.org/10.1007/430_2014_149.

[11] O. Waldmann, *Inorg. Chem.* **2007**, *46*, 10035.

[12] E. Ruiz, J. Cirera, J. Cano, S. Alvarez, C. Loose, J. Kortus, *Chem. Commun.* **2008**, 52–54, https://doi.org/10.1039/B714715E.

[13] F. Neese, D. A. Pantazis, *Faraday Discuss.* **2011**, *148*, 229.

[14] a) G. Christou, D. Gatteschi, D. N. Hendrickson, R. Sessoli, *MRS Bull.* **2000**, *25*, 66; b) K. S. Pedersen, J. Bendix, R. Clérac, *Chem. Commun.* **2014**, *50*, 4396.

[15] N. Ishikawa, M. Sugita, T. Ishikawa, S. Koshihara, Y. Kaizu, *J. Am. Chem. Soc.* **2003**, *125*, 8694.

[16] H. L. Feltham, S. Brooker, *Coord. Chem. Rev.* **2014**, *276*, 1.

[17] R. Ruamps, L. J. Batchelor, R. Maurice, N. Gogoi, P. Jiménez-Lozano, N. Guihéry, C. de Graaf, A.-L. Barra, J.-P. Sutter, T. Mallah, *Chem. Eur. J.* **2013**, *19*, 950.

[18] Y. Rechkemmer, F. D. Breitgoff, M. van der Meer, M. Atanasov, M. Hakl, M. Orlita, P. Neugebauer, F. Neese, B. Sarkar, J. van Slageren, *Nat. Commun.* **2016**, *7*, 10467.

[19] M. Ding, G. E. Cutsail III, D. Aravena, M. Amoza, M. Rouzières, P. Dechambenoit, Y. Losovyj, M. Pink, E. Ruiz, R. Clérac J M Smith, *Chem. Sci.* **2016**, *7*, 6132.

[20] J. M. Zadrozny, D. J. Xiao, M. Atanasov, G. J. Long, F. Grandjean, F. Neese, J. R. Long, *Nat. Chem.* **2013**, *5*, 577.

[21] X.-N. Yao, J.-Z. Du, Y.-Q. Zhang, X.-B. Leng, M.-W. Yang, S.-D. Jiang, Z.-X. Wang, Z.-W. Ouyang, L. Deng, B.-W. Wang S Gao, *J. Am. Chem. Soc.* **2017**, *139*, 373.

[22] A. Sarkar, S. Dey, G. Rajaraman, *Chem. - Eur. J.* **2020**, *26*, 14036.

[23] a) G. Peng, Y.-F. Qian, Z.-W. Wang, Y. Chen, T. Yadav, K. Fink, X.-M. Ren, *Cryst. Growth Des.* **2021**, *21*, 1035; b) L. Smolko, J. Černák, M. Dušek, J. Miklovič, J. Titiš, R. Boča, *Dalton Trans.* **2015**, *44*, 17565.

[24] A. Buchholz, A. O. Eseola, W. Plass, *C. R. Chim.* **2012**, *15*, 929.

[25] D.-K. Cao, J.-Q. Feng, M. Ren, Y.-W. Gu, Y. Song, M. D. Ward, *Chem. Commun.* **2013**, *49*, 8863.

[26] W. Huang, T. Liu, D. Wu, J. Cheng, Z. W. Ouyang, C. Duan, *Dalton Trans.* **2013**, *42*, 15326.

[27] a) Y.-S. Meng, Z. Mo, B.-W. Wang, Y.-Q. Zhang, L. Deng, S. Gao, *Chem. Sci.* **2015**, *6*, 7156; b) G. A. Craig, M. Murrie, *Chem. Soc. Rev.* **2015**, *44*, 2135.

[28] a) A. Cini, M. Mannini, F. Totti, M. Fittipaldi, G. Spina, A. Chumakov, R. Rüffer, A. Cornia, R. Sessoli, *Nat. Commun.* **2018**, *9*, 480; b) S. Gao, *Molecular Nanomagnets and Related Phenomena*, Springer Berlin Heidelberg, Berlin, Heidelberg, **2015**.

[29] a) S. Ziegenbalg, D. Hornig, H. Görls, W. Plass, *Inorg. Chem.* **2016**, *55*, 4047; b) M. Böhme, S. Ziegenbalg, A. Aliabadi, A. Schnegg, H. Görls, W. Plass, *Dalton Trans.* **2018**, *47*, 10861; c) H.-H. Cui, F. Lu, X.-T. Chen, Y.-Q. Zhang, W. Tong, Z.-L. Xue, *Inorg. Chem.* **2019**, *58*, 12555.

[30] A. K. Sharma, J. Kim, J. T. Prior, N. J. Hawco, N. P. Rath, J. Kim, L. M. Mirica, *Inorg. Chem.* **2014**, *53*, 11367.

[31] Y. A. Pankratova, Y. V. Nelyubina, V. V. Novikov, A. A. Pavlov, *Russ. J. Coord. Chem.* **2021**, *47*, 10.

[32] M. Cibian, G. S. Hanan, *Chemistry* **2015**, *21*, 9474.

[33] P. Bertrand, *Electron Paramagnetic Resonance Spectroscopy*, Springer International Publishing, Cham, **2020**.

[34] F. Lloret, M. Julve, J. Cano, R. Ruiz-García, E. Pardo, *Inorg. Chim. Acta* **2008**, *361*, 3432.

[35] D. Reta, N. F. Chilton, *Phys. Chem. Chem. Phys.* **2019**, *21*, 23567.

[36] A. Singh, K. N. Shrivastava, *Physica Status Solidi (b)* **1979**, *95*, 273–277, https://doi.org/10.1002/pssb.2220950131.

[37] *SAINT-V6.28 A. Data Reduction Software*, Bruker, **2001**.

[38] G. M. Sheldrick, *SADABS. Program for Empirical Absorption Correction*, Göttingen, **1996**.

[39] a) L. J. Farrugia, *J. Appl. Crystallogr.* **1999**, *32*, 837; b) G. M. Sheldrick, *SHELXL-97. Program for the Refinement of Crystal*, Göttingen, **1997**; c) G. M. Sheldrick, *Acta Crystallogr. Sect. A* **1990**, *46*, 467.

[40] a) F. Neese, *WIREs Comput. Mol. Sci.* **2012**, *2*, 73; b) F. Neese, F. Wennmohs, U. Becker, C. Riplinger, *J. Chem. Phys.* **2020**, *152*, 224108.

[41] J. Jung, M. Atanasov, F. Neese, *Inorg. Chem.* **2017**, *56*, 8802.

[42] F. Weigend, R. Ahlrichs, *Phys. Chem. Chem. Phys.* **2005**, *7*, 3297.

[43] A. D. Becke, E. R. Johnson, *J. Chem. Phys.* **2005**, *123*, 154101.

[44] K. Eichkorn, F. Weigend, O. Treutler, R. Ahlrichs, *Theoretical Chemistry Accounts: Theory, Computation, and Modeling (Theoretica Chimica Acta)* **1997**, *97*, 119–124, https://doi.org/10.1007/s002140050244.

[45] C. Angeli, R. Cimiraglia, S. Evangelisti, T. Leininger, J.-P. Malrieu, *J. Chem. Phys.* **2001**, *114*, 10252.

[46] M. Reiher, *Theor. Chem. Acc.* **2006**, *116*, 241.

[47] a) L. F. Chibotaru, L. Ungur, *J. Chem. Phys.* **2012**, *137*, 64112; b) L. Ungur, L. F. Chibotaru, *Chem. - Eur. J.* **2017**, *23*, 3708.

[48] H. Lueken, *Magnetochemie. Eine Einführung in Theorie und Anwendung*, Teubner Studienbücher (TSBC), **1999**.

[49] N. F. Chilton, R. P. Anderson, L. D. Turner, A. Soncini, K. S. Murray, *J. Comput. Chem.* **2013**, *34*, 1164.

RESEARCH ARTICLE

A Co(II) based single ion magnet with N_2O_2 donor set shows slow magnetic relaxation in magnetic field. Spin-lattice relaxation from 1.8 to 8 K in 14 different magnetic fields up to 1 Tesla was investigated by AC magnetometry. The results are discussed with respect to *ab-initio* multi-reference CASSCF and qualitative ligand field theory (AILFT) calculations.
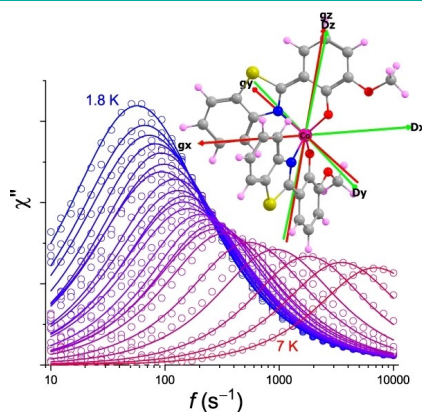
S. Kumar, S. Arumugam, Dr. B. Schwarz*, Prof. Dr. H. Ehrenberg, Prof. Dr. K. C. Mondal*

1 – 12

Static and Dynamic Magnetic Properties of a Co(II)-Complex with N_2O_2 Donor Set – A Theoretical and Experimental Study